CHARACTERISTICS OF A HIGH INTENSITY, PULSED, POTASSIUM VAPOR LASER IN A HEAT PIPE

THESIS

Edward J. Hurd, Jr., Captain, USAF
AFIT/GE/ENG/11-17

DEPARTMENT OF THE AIR FORCE
AIR UNIVERSITY

AIR FORCE INSTITUTE OF TECHNOLOGY

Wright-Patterson Air Force Base, Ohio

AFIT/GE/ENG/11-17

CHARACTERISTICS OF A HIGH INTENSITY, PULSED, POTASSIUM VAPOR LASER IN A HEAT PIPE

THESIS

Presented to the Faculty

Department of Electrical and Computer Engineering

Graduate School of Engineering and Management

Air Force Institute of Technology

Air University

Air Education and Training Command

In Partial Fulfillment of the Requirements for the

Degree of Master of Science in Electrical Engineering

Edward J. Hurd, Jr., BS, MBA

Captain, USAF

March 2011

AFIT/GE/ENG/11-17

CHARACTERISTICS OF A HIGH INTENSITY, PULSED, POTASSIUM VAPOR LASER IN A HEAT PIPE

Edward J. Hurd, Jr., BS, MBA
Captain, USAF

Approved:

Lt Col Jeremy C. Holtgrave (Chairman)	14 Mar 11 Date
Glen P. Perram, Ph.D. (Member)	10 MAR 11 Date
Lt Col Michael R. Hawks (Member)	10 MAR 11 Date

Abstract

This thesis research paper presents the results of experiments using an optically pumped, pulsed potassium vapor laser in a heat pipe. The absorption on the potassium D_2 line, output laser characteristics, and Raman scattering in potassium vapor are discussed. The spectral full width at half maximum (FWHM) of the D_2 absorption line was much greater than predicted values for pressure broadening due to the high number density of potassium atoms and the long path length. At 320°C and 0 torr of helium, the FWHM was 765 GHz. At 100 torr it was 968 GHz. At 200 torr it was 1.12 THz. The analyzed potassium laser output characteristics include the temporal dynamics of the laser cavity, the instantaneous energy efficiencies, and the spin-orbit recycling rates. At 320°C with 2500 torr of helium, a potassium laser with 1.53 MW/cm^2 peak intensity and 8.25% slope efficiency was demonstrated. At 320°C and 0 torr of helium, stimulated electronic Raman scattering occurred in the potassium heat pipe. First and second order Stokes and anti-Stokes lines were visible with energy differences identical to the spin-orbit splitting of potassium.

Acknowledgements

I would like to express my sincere appreciation to everyone who contributed their time and effort to help me complete this research. Thank you to Lt Col Holtgrave for your advice and for pointing me toward the DPAL community; to Dr. Perram for providing nearly unlimited knowledge on lasers; and to Lt Col Hawks, Maj Sulham, Greg Smith, Mike Ranft, and Eric Guild for providing guidance and expertise in the labs. Most importantly, I would like to thank my wife and children for their patience and for being my source of strength throughout my time at AFIT.

Edward J. Hurd, Jr.

Table of Contents

Page

List of Figures

List of Tables

Table Page

CHARACTERISTICS OF A HIGH INTENSITY, PULSED,

POTASSIUM VAPOR LASER IN A HEAT PIPE

I. Introduction

Research Motivation

The first laser was successfully demonstrated fifty years ago by Theodore Maiman at the Hughes Research Lab. Since then, lasers have found their way into nearly every technology. Modern military applications, such as the Airborne Laser (ABL) and Advanced Tactical Laser (ATL), demand high power lasers that are effective on the battlefield but are also portable and energy efficient. The current state of the art megawatt class laser is the chemical oxygen iodine laser (COIL). While it is effective, it also has drawbacks. The COIL requires a Boeing 747 to house the laser, the chemicals, and the optics. It has a logistics trail that includes hazardous materials. Finally, the number of laser shots is limited to the finite amount of chemical stored onboard the aircraft [1].

There are a number of ongoing research projects to develop the next generation megawatt class laser. The primary options include solid state lasers, coherently matched arrays of fiber lasers, and gas phase lasers. The main obstacle to high power solid state lasers, such as the Nd:YAG, is heat control. Heat generated by the laser and pump can cause significant optical aberrations in the lasing crystal. Future power scaling depends on the ability to rapidly cool the crystal during lasing. The coherent matching of fiber

lasers is possible and has been demonstrated. However, the process is technically challenging because the propagation of light is highly dependent on environmental conditions and distance traveled. A large number of highly sensitive wavefront sensors would be required to coherently match the fiber lasers, possibly resulting in poor reliability in the operational environment. The final option, and the motivation behind this thesis, is the gas phase laser. The diode pumped alkali laser (DPAL) is a gas phase laser that combines the advantages of other high power laser options without their respective disadvantages. Its heat control properties are excellent due to the ability of gas to rapidly transfer heat off the lasing axis. The DPAL coherently combines multiple diode laser pump sources without the need for sophisticated wavefront matching. It is capable of fitting in a relatively small volume and requires only electrical power to operate.

Research on DPALs began in 2003 with the successful demonstration of an optically pumped rubidium vapor laser by Krupke [2]. Since then, cesium (Cs), rubidium (Rb), and potassium (K) vapor lasers have been demonstrated and are the subject of research at many institutions across the country. These include the Air Force Research Labs at Kirtland AFB, the Air Force Institute of Technology, the Lawrence Livermore National Laboratory, the United States Air Force Academy, and multiple businesses and universities. Both continuous wave (CW) and pulsed lasers have been studied. There are multiple measures of performance that can be used when analyzing the results of a DPAL demonstration: overall slope efficiency, output intensity over threshold intensity, and total power achieved are the most common. Prior to this thesis research the best slope

efficiency was 82%, the most power achieved was 145 watts CW, and 32 times threshold was the best power scaling achieved [2] [3]. This thesis will focus on the limits of what is possible with a high intensity, pulsed, potassium vapor laser.

II. Literature Review

Laser Physics

An understanding of lasers begins with the laser cavity, which is almost always designed as a stable optical resonator. Stable resonators can be created using two or more flat or curved mirrors. At least one mirror must have a transmittance greater than zero to allow laser light to escape the cavity. These cavities can be analyzed using techniques from geometric optics. According to Verdeyen, the condition for a stable, two-mirror cavity is:

$$\frac{L_c}{R_n} \leq 1 \tag{1}$$

where L_c is the length of the cavity and R_n is the radius of curvature of mirror n [4]. Stable cavities, also known as Fabry-Perot etalons, utilize constructive and destructive interference to allow only a select set of wavelengths to pass through. Figure 1 is a sample plot of this effect. The separation between these transmitted wavelengths, known as the free spectral range (FSR), is:

$$\Delta\upsilon_{\text{FSR}} = \frac{c}{2nL_c} \tag{2}$$

where c is the speed of light and n is the index of refraction. The full width at half max (FWHM) of the transmitted wavelength band is dependent upon the reflectivity of the mirrors by the equation:

$$\Delta\upsilon_{\text{FWHM}} = \frac{\Delta\upsilon_{\text{FSR}}}{F} = \Delta\upsilon_{\text{FSR}} \frac{1 - (\rho_1\rho_2)^{1/2}}{\pi(\rho_1\rho_2)^{1/4}} \tag{3}$$

where ρ_n is the reflectivity of mirror n and F is the Finesse of the cavity.

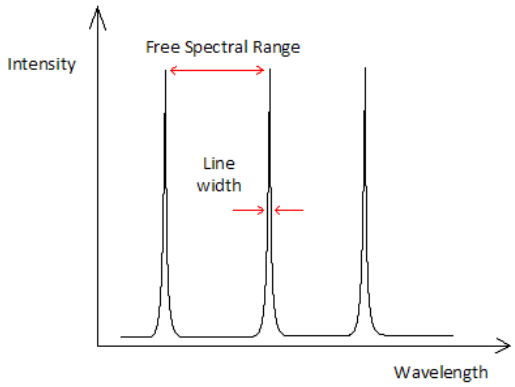

Figure 1. Laser Cavity Etalon Effects.
The FSR is proportional to cavity length and the line width is related to mirror reflectivity.

Most lasers rely on the fact that electrons exist in very specific quantum energy levels in atoms and molecules. In order to achieve lasing, a population inversion between an upper energy level and a lower energy level must be created. The upper state can be pumped using a variety of methods including optical, electronic, and chemical excitation. Figure 2 is a representation of an optically pumped 3-level laser, such as a DPAL. Population in the upper energy levels can be removed through various processes including spontaneous emission of photons, stimulated emission of photons, atomic collisions, quenching, and nonlinear processes. The population in each state at any given time can be modeled as a series of differential equations plus the conservation of atoms equation:

$$\frac{dN_2}{dt} = \frac{\sigma_{20}(\upsilon) I_P}{h\upsilon_{20}}\left[\frac{g_2}{g_1}N_0 - N_2\right] - \frac{N_2}{\gamma_{21}} - \frac{N_2}{\tau_{20}} \tag{4}$$

$$\frac{dN_1}{dt} = \frac{N_2}{\tau_{21}} - \frac{\sigma_{10}(\upsilon) I_L}{h\upsilon_{10}}\left[N_1 - \frac{g_1}{g_0}N_0\right] - \frac{N_1}{\tau_{10}} \tag{5}$$

$$N = N_0 + N_1 + N_2 \tag{6}$$

where N_m is the population in energy level ‹m›, σ_{mn} is the cross section for absorption between ‹m› and ‹n›, I_P is the pump intensity, I_L is the laser intensity, g_m is the degeneracy of ‹m›, τ_{mn} is the radiative lifetime between ‹m› and ‹n›, and γ_{21} is the non-radiative lifetime between ‹2› and ‹1›. Before the pump is turned on, the population is almost entirely in the ground state. Before lasing begins, the spontaneous emission term dominates Equations 4 and 5. Once lasing has begun, this term can be approximated as zero. An accurate picture of laser operation can be realized by solving these equations.

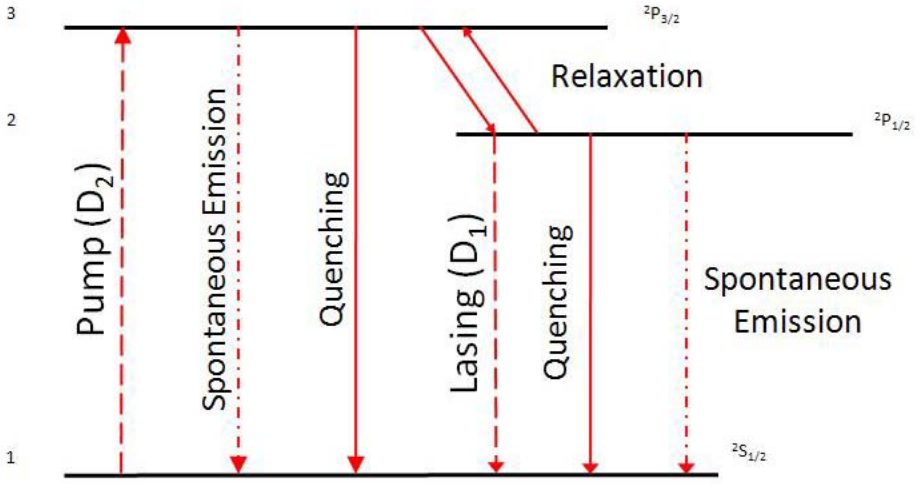

Figure 2. Three-Level DPAL Representation.
This representation of a DPAL system shows optical transitions with dashed arrows and mechanical transitions with solid arrows. Lasing cannot begin until a population inversion has been obtained.

Alkali Metals

With the addition of hydrogen, the alkali metals form the first column of the periodic table. From the top, this column includes lithium, sodium, potassium, rubidium, and cesium. They each have one valence electron, making their quantum energy levels easily calculated and well known. The ground state of the alkali metals is the $^2S_{1/2}$ state.

The first excited energy level has a fine structure with two distinct possibilities for total angular momentum; the $^2P_{3/2}$ and the $^2P_{1/2}$ states. The magnitude of the fine structure splitting is directly related to the strength of the electromagnetic field of the atomic nucleus. Thus, heavier alkalis have a greater spin-orbit splitting than lighter alkalis. Table 1 identifies the various alkali metals and the transition wavelengths to the first excited state. The optical transition between $^2P_{1/2}$ and $^2S_{1/2}$ is known at the D_1 line and the optical transition between $^2P_{3/2}$ and $^2S_{1/2}$ is known as the D_2 line. The energy difference, ΔE, between $^2P_{3/2}$ and $^2P_{1/2}$ is known as the quantum defect. The hyperfine splitting of the alkali metals can be approximated as zero for use in DPALs, leaving $^2S_{1/2}$ and $^2P_{1/2}$ with two degenerate energy levels and $^2P_{3/2}$ with four degenerate energy levels.

Table 1. D_1 and D_2 Transition Wavelengths & Quantum Defects

Alkali	**D_1 Line**	**D_2 Line**	**ΔE**
Li	670.98 nm	670.96 nm	0.34 cm^{-1}
Na	589.76 nm	589.10 nm	17.2 cm^{-1}
K	770.11 nm	766.70 nm	57.7 cm^{-1}
Rb	794.11 nm	780.25 nm	237 cm^{-1}
Cs	894.59 nm	852.35 nm	554 cm^{-1}

The alkali metal potassium, element symbol K, is the subject of this thesis. It is desirable for use in a DPAL because its spin-orbit splitting is large enough to allow for optical pumping on a pressure-broadened D_2 line and small enough to enable very light atoms and molecules to serve as effective collisional partners for spin-orbit relaxation. Potassium is solid at room temperature and must be heated past its melting point of 63.65˚C to produce any considerable vapor concentrations that could be used in a DPAL. After its melting point, the vapor pressure can be found using the following equation:

$$P = 10^{7.4077 - \frac{4453}{T+273.15}} \tag{7}$$

where P is the pressure in mbar and T is the temperature in ˚C [5]. The density of potassium atoms can then be calculated using the ideal gas law:

$$n = \frac{P * 133.322}{k_B * (T + 273)} * \frac{1}{10^6} \tag{8}$$

where n is the density in cm^3 and k_B is the Boltzmann constant. Potassium has an average atomic mass, m, of 6.492×10^{-26} kg. The radiative lifetime, τ_R, of the first excited state is 26.37 ns and the natural line width, $\Delta\nu_N$, is 6.035 MHz.

In addition to natural broadening, the line shape of the D_1 and D_2 transitions are affected by a combination of Doppler broadening and pressure broadening. Doppler broadening occurs as a result of potassium atoms moving parallel to the pump path. The wavelength of the incident radiation is modified slightly by the Maxwellian velocity distribution of the individual atoms. Doppler broadening results in an inhomogeneous line shape that is dependent upon temperature. The follow equations describe the resulting Gaussian profile:

$$g_D(\lambda) = \frac{1}{\lambda_0}\left[\frac{mc^2}{2\pi k_B(T + 273.15)}\right]^{1/2} \mathrm{e}^{-\left[\frac{mc^2(\lambda-\lambda_0)^2}{2k_B(T+273.15)\lambda_0^2}\right]} \tag{9}$$

$$\Delta\lambda_D = \sqrt{\frac{8k_B T \ln(2)}{mc^2}}\lambda_0 \tag{10}$$

where λ_0 is the center wavelength of the transition and m is the average atomic mass. At an operating temperature of 320˚C, the Doppler broadened full width at half max, $\Delta\nu_D$, is 1.09 GHz on the D_2 line, as seen in Figure 3.

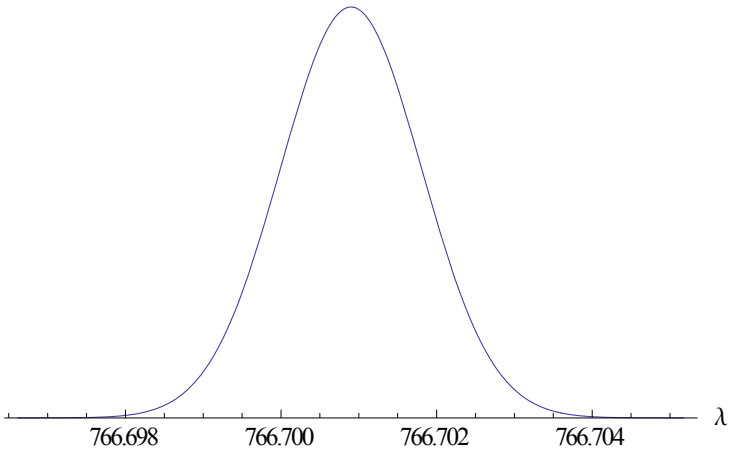

Figure 3. Doppler Broadening of the D_2 Line.
The FWHM of 1.09 GHz is calculated at 320ºC and does not include natural or pressure broadening.

Buffer Gasses

Every DPAL uses one or more buffer gasses to perform two important functions: pressure broaden the D_2 transition and collisionally relax the alkali atoms from the $^2P_{3/2}$ state to the $^2P_{1/2}$ state. Pressure broadening is caused by collisions between the alkali atoms and its neighboring atoms and molecules. It results in a homogenous line shape that is dependent upon the number densities of the collisional partners. The following equations describe the resulting Lorentzian profile for natural broadening plus pressure broadening:

$$g_H(\lambda) = \frac{\Delta\lambda_{\mathrm{H}}/2}{\frac{\pi c}{\lambda^2}\left[(\lambda-\lambda_0)^2 + \left(\frac{\Delta\lambda_{\mathrm{H}}}{2}\right)^2\right]} \tag{11}$$

where

$$\Delta\lambda_H = \left(\frac{\lambda^2}{\mathrm{c}}\right)\Delta\upsilon_{\mathrm{H}} = \frac{\lambda^2}{2\pi c}\left(\frac{1}{\tau_R} + \sum_i k_i P_i\right) \tag{12}$$

where P_i is the partial pressure of the i^{th} collisional partner and k_i is its collisional broadening rate with the alkali atoms [6]. At 200 torr of helium pressure, the D_2 absorption line of potassium vapor is broadened by 2.41 GHz, as seen in Figure 4.

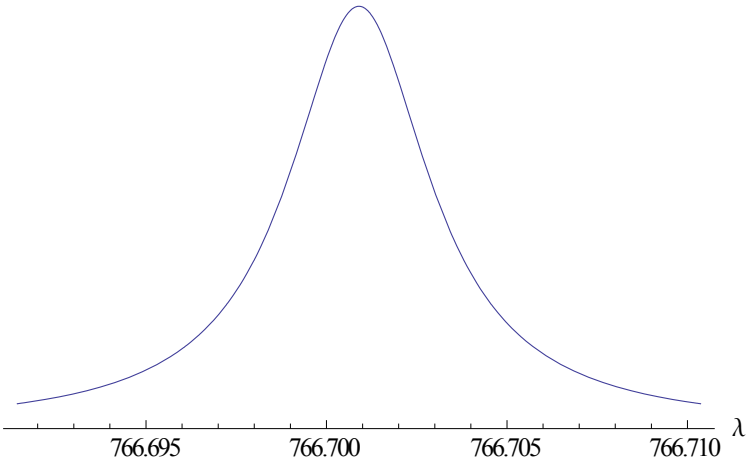

Figure 4. Pressure Broadening of the D_2 Line
The FWHM of 2.41 GHz is calculated at 200 torr of helium and does not include Doppler broadening.

Spin-orbit relaxation, also known as fine structure mixing, is essential to the operation of DPALs. When the spin-orbit rate is faster than the lifetime of the $^2P_{3/2}$ state, the atoms will collisionally relax to the $^2P_{1/2}$ state rather than decay to the ground state. When the population of alkali atoms in this upper lasing state is greater than the population in the ground state, the population inversion required for lasing has been created. The collisional relaxation rate, γ, depends upon the following equations:

$$\gamma_{P_{3/2}\rightarrow P_{1/2}} = n_{gas}\sigma_{P_{3/2}\rightarrow P_{1/2}}V_r \tag{13}$$

where

$$V_r = \left[\frac{8k_BT}{\pi}\left(\frac{1}{m_{alkali}}+\frac{1}{m_{gas}}\right)\right]^{1/2} \tag{14}$$

and where n_{gas} is the concentration of buffer gas in the cell, $\sigma_{P_{3/2}\rightarrow P_{1/2}}$ is the cross section specific to the collisional partners, and V_r is the average relative velocity of the collisional partners, based on a Maxwellian speed distribution.

Buffer gasses serve an additional purpose in DPALs; they move excess heat from lasing and atomic collisions off the lasing axis. When the pump laser is turned on, the temperature immediately begins to rise in the path of this beam. Unchecked, this would create a pressure differential that would significantly reduce the number of alkali atoms available for lasing. In addition to efficiently moving this excess heat, the buffer gas also serves as a barrier to alkali atom migration. This barrier helps to maintain a significant concentration of alkali atoms on the lasing axis. There is a tradeoff when selecting the best buffer gas. Light buffer gasses will have greater relative velocities and move excess heat off the lasing axis quicker than heavy gasses. However, heavy buffer gasses will serve as better barriers to alkali migration.

The buffer gasses useful for spin orbit relaxation are limited to those inert gasses that will not chemically react with the alkali vapor. The most common candidates are the noble gasses and molecules such as ethane. The cross section for spin-orbit coupling is a measure of the probability that an alkali atom and buffer gas will collide and relax the alkali from the $^2P_{3/2}$ state to the $^2P_{1/2}$ state. These values vary greatly between collisional partners. As shown in Equation 14, temperature also plays an important role in the overall spin-orbit relaxation rate. The cross sections in Table 2 were measured at 95°C and the spin-orbit rate was calculated using Equations 13 and 14 [7].

Table 2. Spin-Orbit Relaxation Gasses

Collision Partner	Cross Section	S.O. Rate (100 torr)
He	40.8 ± 2.1 Å^2	1.57 GHz
Ne	9.45 ± 0.68 Å^2	190 MHz
Ar	22.4 ± 1.6 Å^2	369 MHz
Kr	40.7 ± 1.8 Å^2	577 MHz
Xe	72.3 ± 2.2 Å^2	965 MHz

Heat Pipe Theory

The math and physics of a DPAL system are straight forward, but the actual implementation and demonstration of a working system reveals many engineering problems that must be solved. First, the alkali needs to be confined in order to avoid chemical reactions with the atmosphere. The alkali then needs to be heated to high temperatures in order to achieve higher vapor pressures. This heating will limit the types of materials that can be used to construct an alkali cell. Any cold spots on the cell, such as the optical windows, will cause the alkali to condense. This heating and cooling will eventually move the alkali away from heating element and could potentially obscure the optical windows. Adding high pressures of buffer gasses will put additional physical stresses on the cell. The solution to these problems is the heat pipe shown in Figure 5.

The heat pipe is designed to confine the alkali vapor to the center of the cell without physically touching the optical windows or the buffer gas inlets which would normally act as the cold points. Solid potassium placed at the center of the heat pipe is heated to some temperature above the melting point. The resulting potassium vapor flows upward and outward towards the optical windows. As it approaches the cold blocks, which are held at some temperature below the melting point, the vapor condenses back to its liquid form. A wicking material installed along the edges of the heat pipe

pulls the potassium back towards the center of the heat pipe where the process begins again.

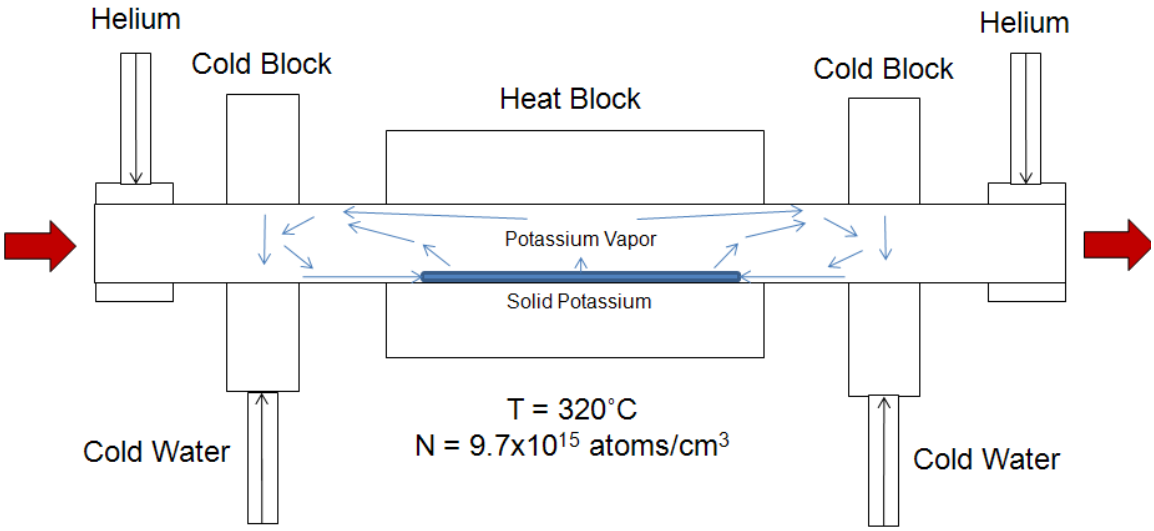

Figure 5. Heat Pipe Theory.
Solid potassium is heated to form a vapor which then moves away from the heat source. At the cold blocks, it condenses to a liquid and is wicked back towards the center.

Raman Scattering

When a photon collides with an atom or molecule, it can either be absorbed or scattered. There are three known types of scattering: Raleigh, Brillouin, and Raman. Raleigh scattering can be described as the elastic absorption and reemission of a photon and accounts for the vast majority of scattered light under normal conditions. This process may redirect the photon but does not change its energy. Brillouin scattering is the inelastic scattering of a photon from a medium with a fluctuating density gradient. The photon can either gain or lose energy during this process through the absorption or emission of phonons, magnons, or other sources of quantized energy. Raman scattering

is the inelastic scattering of a photon between rotational, vibrational, and/or electronic energy states. Stokes transitions occur when a photon is absorbed in a lower energy state and relaxes back to a higher state, yielding a new photon that is lower in energy by the difference in energy between the two states. Anti-Stokes transitions occur when the opposite happens, yielding a photon with more energy than the original. Figure 6 is a visualization of Rayleigh and Stokes scattering from a diatomic molecule.

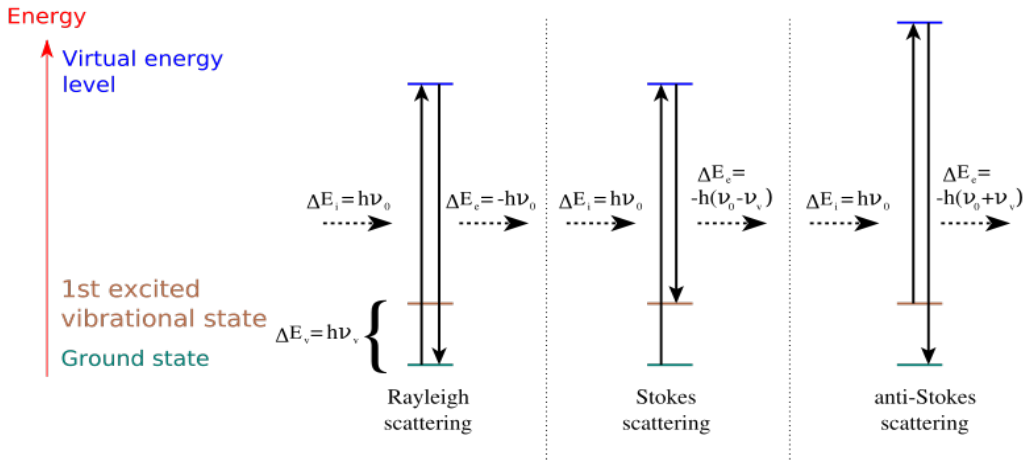

Figure 6. Elastic and Inelastic Photon Scattering.
Rayleigh scattering is elastic and does not change the incident photon's energy. Raman scattering is inelastic and can yield a photon with more or less energy than the original [15].

Stimulated Raman scattering (SRS) occurs when the Stokes or anti-Stokes transition is initiated by a signal photon. The energy from an incident pump photon is transferred into a new signal photon that exactly matches the phase and direction of the original signal photon. This process is similar in nature to stimulated emission, from which lasers are possible. However, since the upper laser state is a virtual energy level, there is no requirement for a population inversion. Raman lasers and optical amplifiers in fiber optic cables can be readily created using SRS.

III. Methodology

Experimental Setup

The general purpose of the experiments detailed in this thesis was to characterize the performance of a high intensity, optically pumped, pulsed potassium vapor laser in a heat pipe. There were three separate experiments that each utilized the same general setup: the D_2 absorption feature experiment, the K-DPAL experiment, and the SRS experiment. Figure 7 is a layout of the relative positions of equipment installed on the optics table. The purpose of each item along the laser path will be explained in this section.

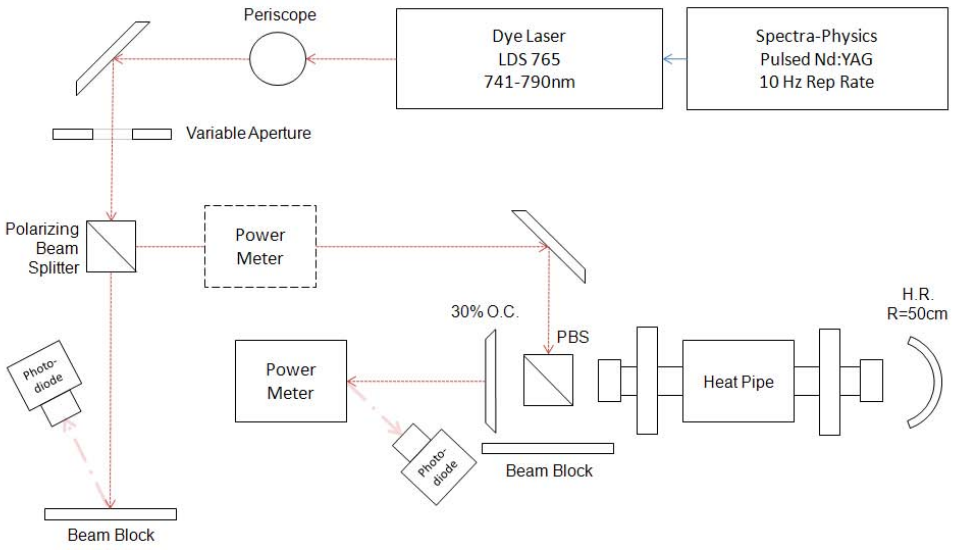

Figure 7. Experimental Setup.
The K-DPAL system is pumped by a tunable dye laser with a 5 to 8 ns pulse. The pump beam is coupled into the stable laser cavity using a polarizing beam splitter. The output laser is measured with a power meter, a photodetector, and a spectrometer.

The laser pulse began with a Spectra-Physics Quanta-Ray Nd:YAG laser frequency doubled to 1064 nm. It was a Q-switched type laser which operated at a 10 Hz repetition rate. This laser was used to pump a Sirah PRSC-D-18 pulsed dye laser containing the LDS765 solution. This dye produced its peak power very close to the potassium D_2 transition and had a usable range between 741 and 790 nm. The wavelength emitted by the dye laser was selected by two 90 mm, 1800 lines/mm gratings. The dye laser cavity was open to the atmosphere and the selected wavelength compensated for the index of refraction of air, $n = 1.000293$. The spectral line shape produced by this grating had a FWHM of approximately 31 GHz and sat on a spectral plateau that was up to 4 nm in width [8]. From this point on, the output of the dye laser will be referred to as the pump laser. The pump laser traveled through a low-loss periscope to be positioned exactly 6" above the optics table. A flat high reflecting mirror, M_1, directed the beam through a variable aperture fixed at 5.0 mm in diameter. The aperture was aligned such that the hot spot of the pump laser was allowed to pass while most of the wings were blocked. The spot size of the pump laser was highly dependent upon output power. The aperture eliminated this variable, leaving it a constant for varying pump powers.

The spatially controlled pump laser was incident on a polarizing beam splitter, PBS_1. A small fraction of the light passed through the PBS and scatted off a beam block. The temporal pulse shape of this scattered radiation was detected by a New Focus Model 1621 visible nanosecond photodetector and recorded on a LeCroy Wavepro7300 3 GHz oscilloscope. The recorded pulse shapes were the convolution between the actual pulse

shape and the system impulse response. The majority of the pump laser was reflected off the PBS and traveled in the direction of the DPAL cavity. At this point, a Coherent Powermax PM30 power meter was moved into position to detect the time-averaged power incident on the laser cavity. When this power meter was not blocking the beam, the pump laser reflected off another flat mirror, M_2, and entered the laser cavity through a second beam splitter, PBS_2.

The laser cavity consisted of a flat 30% output coupler (OC), PBS_2, the heat pipe, and a high reflector (HR) with a 50 cm radius of curvature. The optical windows at either end of the heat pipe each had approximately an 8% loss. The heating element was a large aluminum block driven by a Watlow SD6C temperature controller using eight C1E14-L12 heater cartridges and a thermocouple-controlled switch. The cooling elements were smaller aluminum blocks that used cold flowing water supplied by a pair of Neslab RTE-111 chillers. The inlet valves on the heat pipe were connected to a plumbing system that allowed the cell to be vacuum pumped or to be pressurized with one or more buffer gasses.

Any light that passed through the OC could be measured in three different ways: a Coherent Powermax PM10 power meter displayed the time-averaged output power, an Ocean Optics HR4000CG spectrometer recorded the spectral frequencies of the output onto a laptop, and a second photodetector recorded the temporal pulse shape onto the oscilloscope. The first photodetector served as the trigger for the second.

Procedures

The following procedures were used to align the optical components for each of the experiments conducted for this thesis. Before the laser cavity optics were positioned, a helium neon (HeNe) laser was installed approximately 30 cm behind the HR. The HeNe was precisely aligned to pass straight through the center of the heat pipe and remain perfectly level at 6" above the optics table. PBS_2 was installed such that the reflection of the HeNe fell back upon the source. The 30% OC was also aligned using its reflection. When the curved HR was installed, it yielded two reflections: one from each surface. By aligning both reflections back on the source, the HR could be perfectly centered on the laser axis. External to the laser cavity, the HeNe light passing through the OC was used to center the power meter on the expected path of the K-DPAL. The HeNe laser reflected off PBS_2 was steered using M_2 to strike the center of PBS_1. Unlike the visible HeNe laser, the pump laser had to be aligned using an infrared (IR) card. Using M_1, the pump laser was steered to the center of PBS_1. Finally, by holding the IR card just in front of the HR, the fine controls on the mount for PBS_1 could be used to precisely align the pump laser with the HeNe laser. With the HeNe laser securely installed on the optics table, realignment of the DPAL system could be accomplished at any time with minimal effort.

The following tasks were used at various times to prepare the potassium heat pipe for data collection. To give enough time for the heat pipe to reach the desired operating temperature, the heater and chillers were turned on at least one hour before collecting data. The thermocouple connection on the Watlow controller was not wired correctly, so

a J-type thermocouple was connected to a calibrated HH506 Multilogger thermometer for a much more accurate temperature reading. The accuracy of the J-type thermocouple at the operating temperatures used in these experiments was ±2.2ºC [9]. To prevent possible contamination, the heat pipe inlet valves were only opened when adding or removing buffer gas. In order to minimize the loss of potassium atoms, the vacuum pump was used to reduce buffer gas pressure only when the temperature was below the melting point of potassium. Buffer gas could be added at any operating temperature by opening the inlet valves and using a separate needle valve plumbed into the system to control the flow. An MKS Baratron 15000 torr pressure transducer measured the pressure at a point just outside the inlet valves. The error for this transducer was ±0.15 torr. If the cell was already heated when buffer gas was added, the new sample required 10 to 15 minutes to stabilize.

Data Collection

The procedures to collect data for the D_2 line absorption feature experiment are discussed in this paragraph. The general experimental setup detailed in Figure 7 was modified by replacing the curved high reflector with the PM30 power meter. This setup allowed for the measurement of the transmittance of a single pass of the pump laser. To gather data points across the D_2 absorption line, the pump laser was manually scanned between 764 and 769 nm in increments of 0.2 nm. Increments of 0.1 or 0.05 nm were also used when appropriate to maintain the resolution of the data. The pump laser was set to its minimum power setting and the input and output power values were recorded for each incremental wavelength. Prior to heating the potassium or adding any buffer

gas, a dataset was collected to quantify the baseline optical losses of the laser cavity. This would be useful in characterizing the laser performance and pump absorption. The heat pipe was then heated to 320°C and data was collected at buffer gas pressures of 0, 100, and 200 torr of helium. No pulse shape or spectroscopic emission data was collected for this experiment.

The procedures to collect data for the K-DPAL experiments are discussed in this paragraph. The pump laser was set at a wavelength of 766.923 nm to account for the index of refraction of air in the dye laser cavity. The pulse shape data was collected using one of the photodetectors and averaged over 30 seconds on the oscilloscope, which equated to 300 actual laser pulses. Saturation of the photodetectors occurred at approximately 1.4 V as displayed on the oscilloscope. In order to get the largest signal possible without the effects of saturation, the final averaged pulse shape had to have an amplitude between 1.3 and 1.4 V. Pulse shapes that did not meet this criterion were rejected and recompleted. The pump laser pulse shapes were recorded using a 300 sample dataset for each of the five amplifier settings on the Nd:YAG. The output from the power meters was recorded manually. The spectroscopic emission data was recorded onto the laptop using a 10 ms integration time. The laptop was also used to ensure the system was actually being pumped on the D_2 line and lasing on the D_1 line. The heat pipe was heated to 320°C and data was collected at buffer gas pressures of 0, 100, 200, 500, 1000, 1400, 2000, and 2500 torr of helium.

The procedures to collect data for the stimulated Raman scattering experiments are discussed in this paragraph. The purpose behind this experiment was to further

analyze the unidentified emission line detected during the K-DPAL experiments when no buffer gas was present in the system. The same experimental setup and data collection strategy was used, but the dye laser was programmed to scan between 760 and 780 nm, which covered both the D_1 and D_2 lines. The spectrometer was setup to record the resulting emissions in 0.1 nm increments while the dye laser was running the scan.

IV. Results and Analysis

D_2 Absorption Feature

The Doppler broadening, Figure 3, and pressure broadening, Figure 4, line shapes of the potassium D_2 transition were calculated independent of path length and number density. These curves could be considered probability distributions for the absorption of incident radiation at those wavelengths. When path length and/or number density became extremely large, the probability of absorption far into the wings of the distribution curves actually became quite significant. When the heat pipe was heated to 320°C, the number density of potassium atoms increased to as much as 9.7×10^{15} atoms/cm^3. Given the spot size of the pump laser and the estimated path length containing potassium vapor, there were up to 2.85×10^{16} atoms in the pump laser's path.

The results of the D_2 absorption feature experiment indicate that the potassium vapor was absorbing photons that were relatively far from the transition's center wavelength. With no helium added to the system, and thus no significant pressure broadening, the FWHM was 765 GHz, a factor of 769 over the calculated Doppler broadening of 1.09 GHz. Add 200 torr of helium and the FWHM increased to 1.12 THz, a factor of 464 over the calculated pressure broadening of 2.41 GHz. These line widths, shown in Figure 8, may seem unreasonable, but preliminary work by Dr. Gordon Hager has confirmed the order of magnitude of these values [10]. Hager's model, shown in Figure 9, was based on the following key assumptions: a Gaussian pump beam, a longitudinally averaged population density, and a pressure broadened system. In reality,

the pump beam had a significant hot spot and the longitudinal distribution of the population density was unknown.

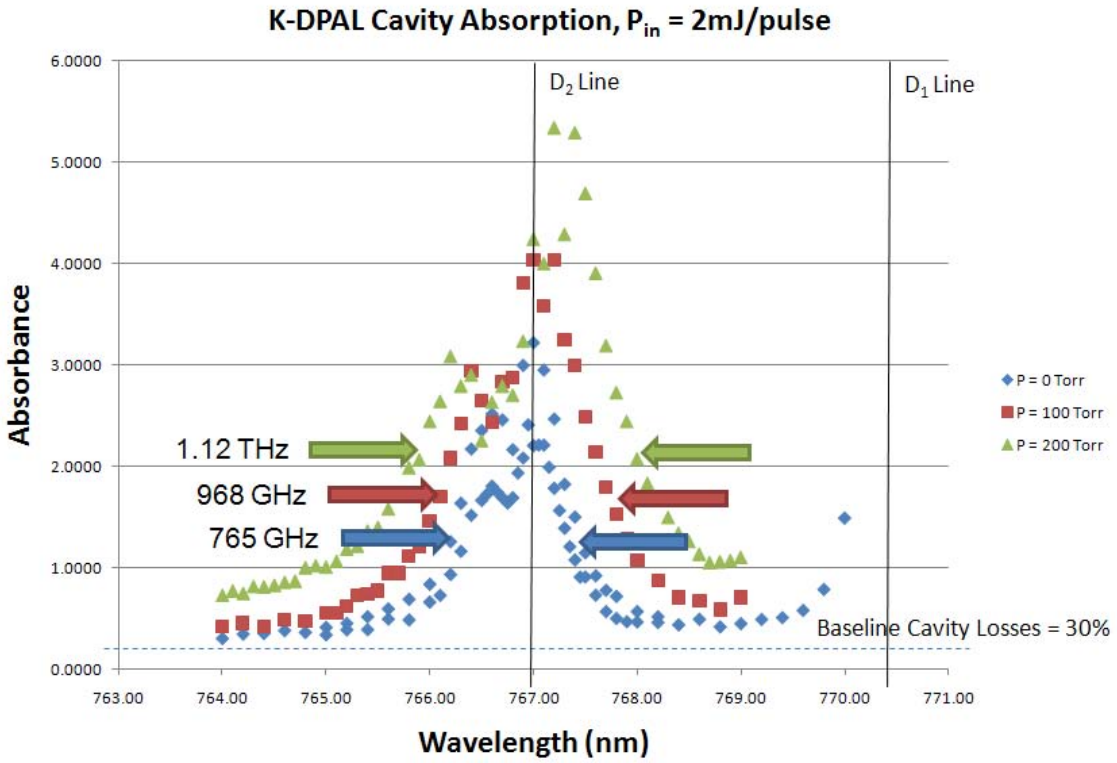

Figure 8. Experimentally Obtained D_2 Line Shapes.
Due to the large concentration of potassium vapor and the long path length of the pump laser, the absorption line width is extremely large, even for relatively low pressures of helium.

These results yield two potential impacts to the overall DPAL effort. One potential advantage is that DPAL systems utilizing large number densities and high buffer gas pressures could use commercial off-the-shelf (COTS), high power diode lasers to pump the system. The highly broadened D_2 line would absorb photons not normally available to DPALs using small number densities and low pressures. This would eliminate or reduce the need for the research and development of narrow-band, high

power diode lasers. One potential disadvantage for the K-DPAL is that the potassium D_1 and D_2 absorption lines could begin to overlap, causing the pump laser to excite the potassium atoms to both the $^2P_{3/2}$ and $^2P_{1/2}$ states simultaneously. This would degrade the population inversion necessary for lasing to occur. Fortunately, the cesium and rubidium DPALs have much greater spin-orbit energy differences and would not be vulnerable to this effect.

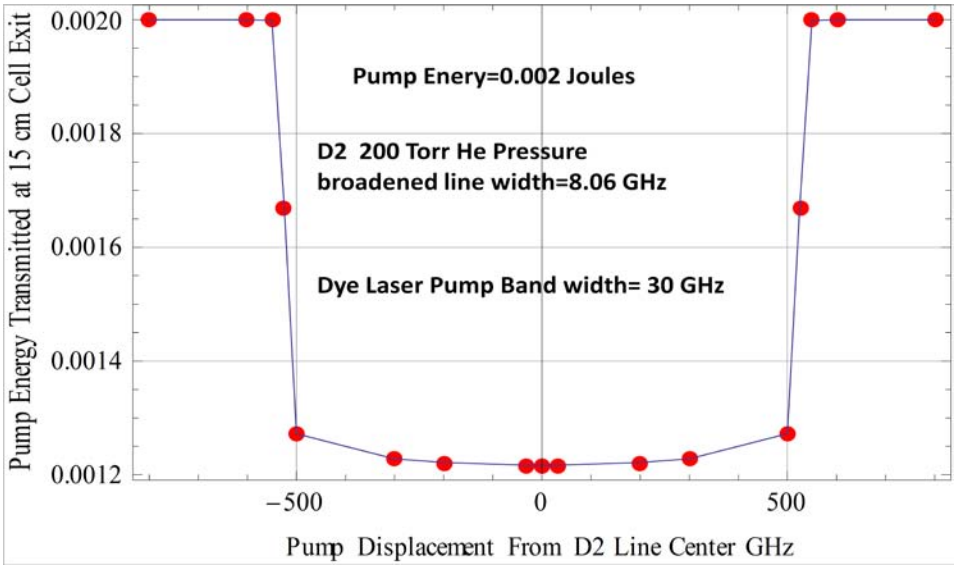

Figure 9. Simulated D_2 Line Shape.
Given the K-DPAL operating parameters, Hager's computer model calculated the D_2 absorption line width at over 1 THz, verifying the experimental results in order of magnitude [10].

Pulse Shape Dynamics

For these experiments, six different pump laser power levels were used and each delivered an increasing amount of energy to the system. The duration of these pump laser pulses was dependent upon the pump power. The corresponding pump pulse energies, durations, and peak powers are listed in Table 3. The pulse shape for each

pump power is shown in Figure 10. The average pulse duration was 7.0 ns and the cavity round trip time was 3.0 ns. Both of these values had a significant impact on the temporal dynamics of the resulting K-DPAL. In a CW laser, the balance between pump input and laser output involves a steady state distribution among the available energy states. However, in this short-pulsed K-DPAL, there was not enough time to reach steady state. In order to achieve lasing, the potassium vapor had to be fully bleached along the lasing axis. Bleaching occurred when every atom that could absorb a pump photon had done so. This could be considered the lower limit for the threshold pump intensity of this K-DPAL. Bleaching the cell was easily accomplished as the pump pulse had many orders of magnitude more photons than there were potassium atoms in the beam path.

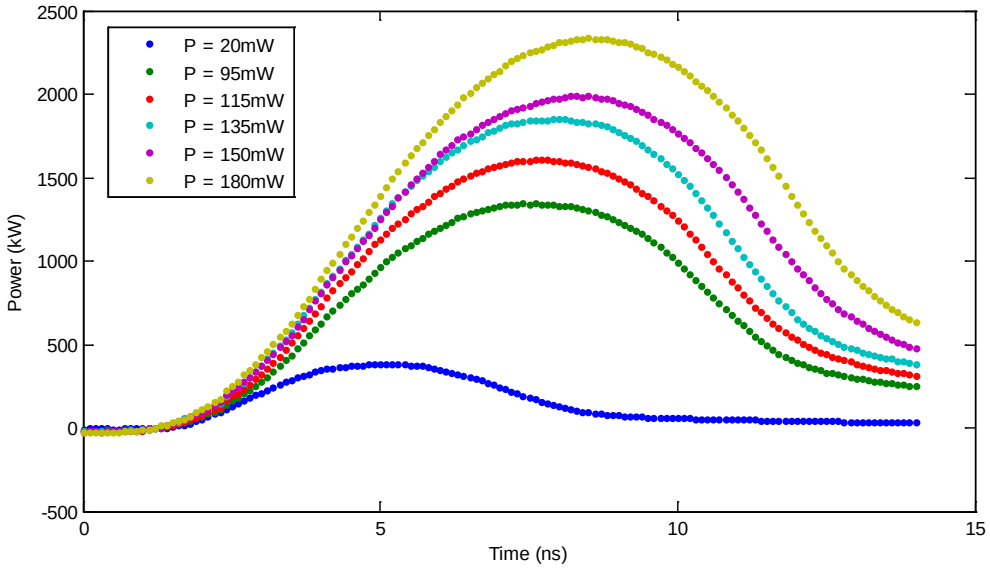

Figure 10. Pump Laser Pulse Shapes.
When the amplifier on the Nd:YAG was turned on, a large step-up in pump power and pulse duration occurred. When the amplifier was tuned higher, there were modest increases in power and duration.

Table 3. Pump Laser Pulse Properties

Time-Avg Pump Power	**Energy Delivered**	**Pulse Duration**	**Peak Power**
20 mW	2.0 mJ	5.1 ns	1.95 MW/cm^2
95 mW	9.5 mJ	6.8 ns	6.85 MW/cm^2
115 mW	11.5 mJ	6.9 ns	8.19 MW/cm^2
135 mW	13.5 mJ	7.1 ns	9.42 MW/cm^2
150 mW	15.0 mJ	7.2 ns	10.1 MW/cm^2
180 mW	18.0 mJ	7.4 ns	11.9 MW/cm^2

As the pump pulse propagated through the laser cavity, it immediately began to shape the outgoing K-DPAL pulse. Figure 11 is a visual aide to the following theoretic description of the temporal dynamics of this K-DPAL system. A few key assumptions were needed to develop this theory: 1) there were significantly more pump photons than could be absorbed by the potassium vapor, 2) the spin-orbit relaxation rate was much faster than spontaneous emission, and 3) there were no losses or other nonlinear effects such as changes of the index of refraction in the gain medium. At point A and time $t = 0$ ns, the pump pulse entered the section of the heat pipe containing potassium vapor. As the pump pulse was absorbed, the atoms were relaxed to the $^2P_{1/2}$ state and spontaneous emission on the D_1 line began to occur in 4π steradians. As the wavefront reached point B, the cell became fully bleached. Photons emitted on the D_1 line could then be amplified through the entire gain medium. Those photons with the correct polarization that were also traveling along a stable optical path, as determined by the cavity mirrors, were returned to the system by the OC for amplification. After one round trip through the laser cavity, the K-DPAL was considered activated and could be measured by the photodetector. Given the length of the pump pulse, there was enough time for only two round trips through the cavity. Furthermore, the pump laser was

reflected off the HR and focused to a point near the center of the gain medium. Additional pump photons could be absorbed during this period of reverse propagation. When the end of the pump pulse passed back through point A, no more energy could be added to the system. The population inversion rapidly diminished after this point.

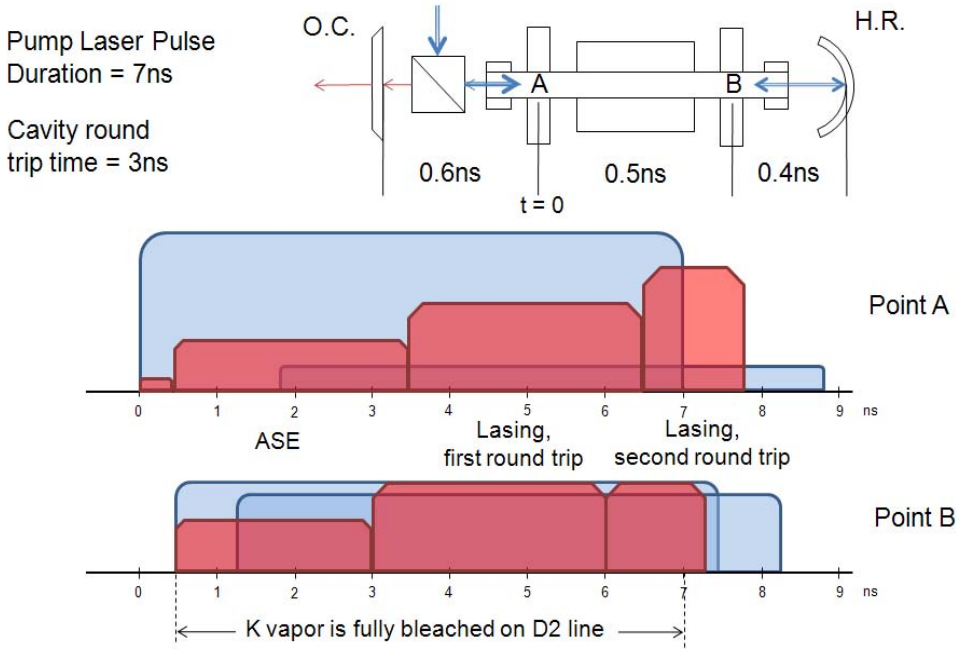

Figure 11. Pump Pulse Propagation through the Laser Cavity. The pump pulse enters point A at t = 0. ASE in 4π steradians begins immediately and lasing begins after the cavity round trip time.

Buffer gas pressure had a direct impact on the K-DPAL, both on the pulse shape and on the total energy per pulse. The pulse shape was determined by the temporal dynamics described in the previous paragraph. Figure 12 shows the pulse shapes for each helium pressure using 95 mW of pump power. The gentle rise between $t = 0$ and 3 ns was likely the result of amplified spontaneous emission visible to the photodetector and may have also contained a relaxation oscillation. The two intensity peaks corresponded

to the first and second round trips through the gain medium. The slope of the trailing edge was slightly less than the leading edge, indicating a gradual rather than instantaneous shutoff of the gain medium. The shallow slope after the trailing edge was an artifact of the system response and could not be eliminated from the results. The relative height of the second peak increased with helium pressure, indicating that more gain was available for the second round trip. This is likely due to an increased ability to absorb photons from the focused, counter-propagating pump pulse.

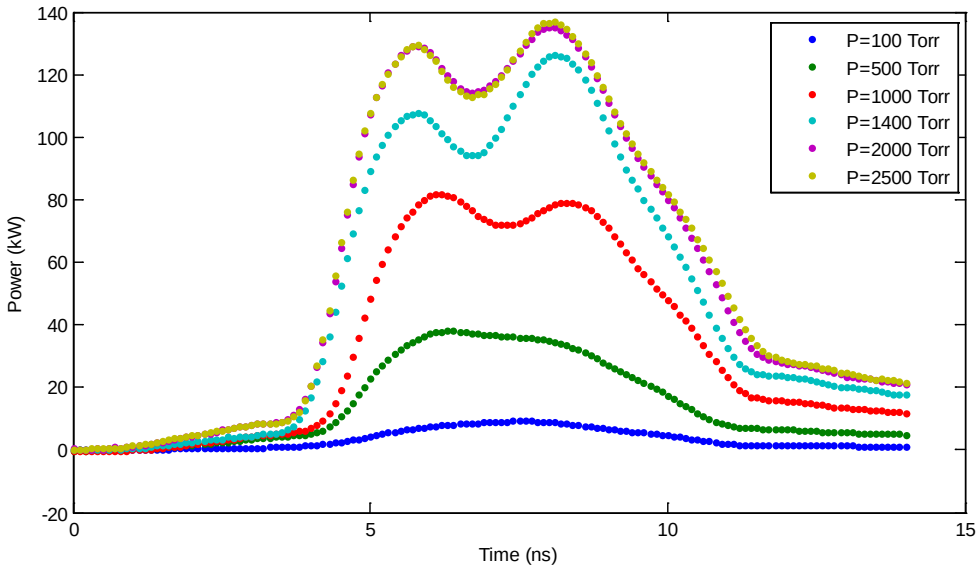

Figure 12. K-DPAL Pulse Shape vs. Helium Pressure.
This dataset was collected using 95 mW of pump power. The output intensity increased with pressure until a maximum was reached. Increased intensity was possible with high pump powers.

For a constant buffer gas pressure, the K-DPAL pulse shape was also affected by the pump power. Figure 13 shows how the second peak grows in proportion to the first peak with increasing pump power. At the lowest pump power setting of 24 mW, the pump pulse duration was only 5.0 ns. This was not enough time to allow for two round

trips through the laser cavity. Thus, there was no second peak on the K-DPAL at 24 mW. Since the pump pulse duration increased with pump power, the time available for gain also increased. This led to a steady increase in the relative magnitude of the second peak.

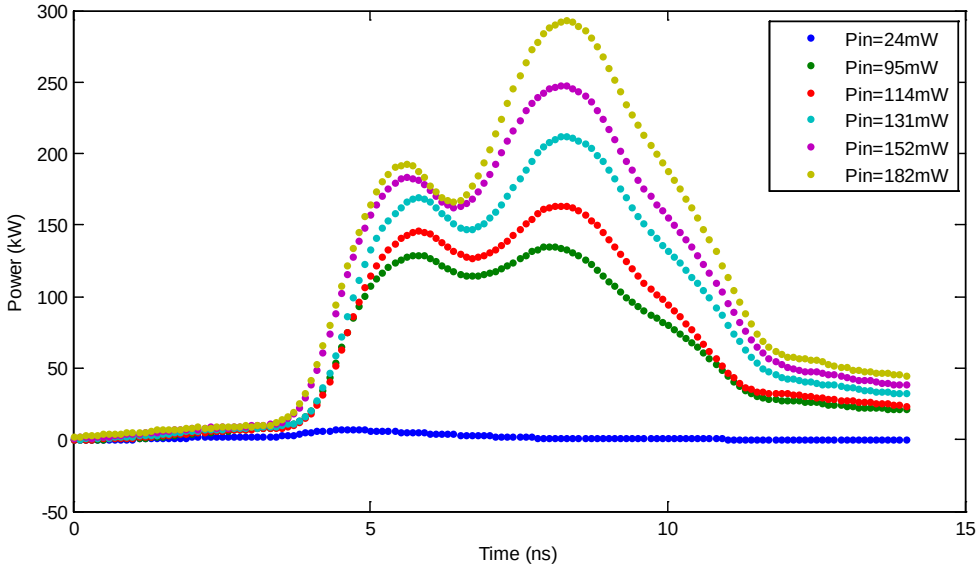

Figure 13. K-DPAL Pulse Shape vs. Pump Power.
The pulse shapes for the 2000 torr of helium dataset show the progression of the second intensity peak with increasing pump power.

K-DPAL Power Efficiency

Measuring the power efficiencies of the experimental data was an important first step in the analysis of this K-DPAL. Two important characteristics of the laser gain medium were estimated using simple linear regression on the data. The slope of the resulting line was the quasi two-level limit for K-DPAL efficiency, which was approximately 11.25%. The x-intercept was the threshold intensity for lasing, which was

approximately 1.22 MW/cm^2. This data can be found in Figure 14. While this method worked for a quick analysis of the data, it is better suited for CW applications.

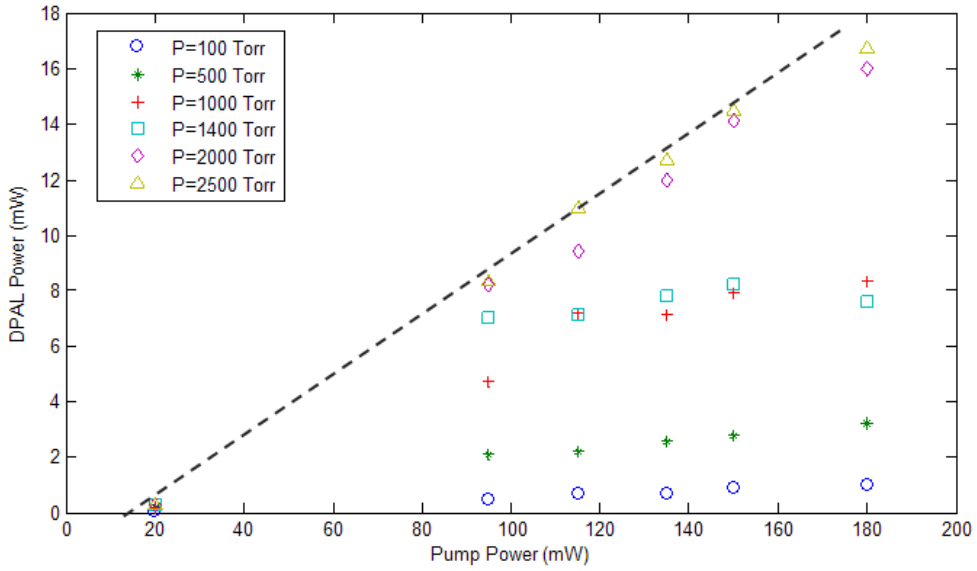

Figure 14. K-DPAL Average Power Efficiency.
The output power of the K-DPAL was directly dependent upon helium pressure. A quasi two-level limit of 11.25% and threshold intensity of 1.22 MW/cm^2 can be estimated from this plot.

A more accurate measure of the slope efficiency for this pulsed laser was the plot of pump pulse power versus K-DPAL pulse power at discrete moments in time. A comparison of efficiencies from each method is provided in Table 4. The key to generating an accurate plot of the instantaneous efficiency was to match the leading edge of the K-DPAL pulse with the leading edge of the pump pulse. While this was not what physically happened in the laser cavity, it was appropriate for this analysis because it aligns the transfer of energy from the pump to the K-DPAL. The time constant, T_c, for the delay between these two points was determined through trial and error. Figure 15

shows how the selection of T_c can modify the resulting plots. The actual time constant for each dataset varied slightly with helium pressure and pump power, but it was always very close the cavity round trip time. These results also support the temporal dynamics theory previously discussed.

Table 4. K-DPAL Efficiencies at 95 mW Pump Power

Helium Pressure	**Average Efficiency**	**Instantaneous Efficiency**
100 torr	0.53%	0.75%
200 torr	0.94%	1.25%
500 torr	2.21%	3.00%
1000 torr	4.95%	7.00%
1400 torr	7.37%	9.75%
2000 torr	8.63%	8.25%
2500 torr	8.74%	8.25%

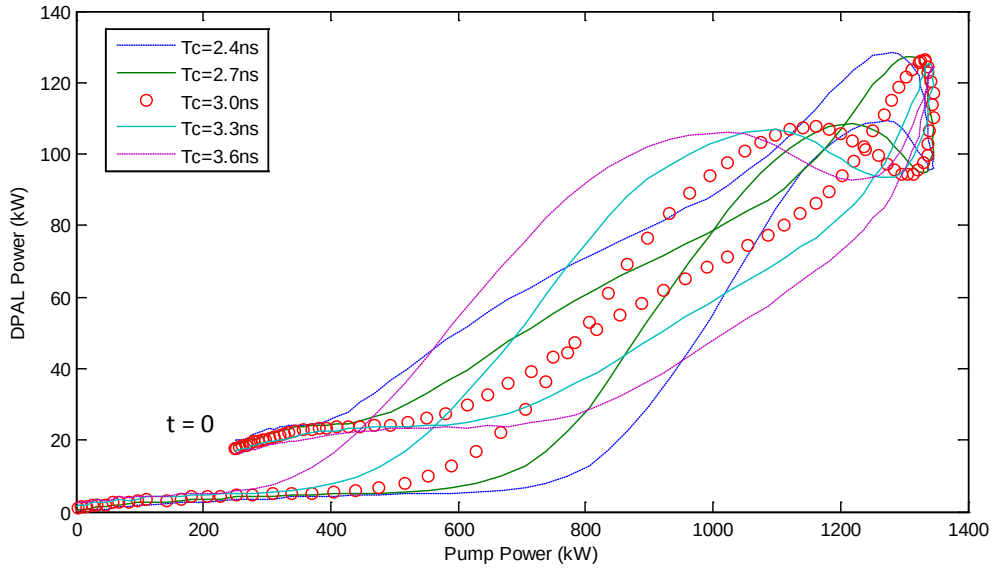

Figure 15. Instantaneous Efficiency vs. Selected Time Constant. Each time constant yielded a different curve. When T_c was close to the cavity round trip time, the curve fell back upon itself.

The instantaneous efficiency plots were difficult to analyze because there were a few features that did not exist in previous pulsed DPAL work accomplished by Cliff Sulham [3]. As displayed in Figure 16, the pulse duration used in that experiment was long enough for a quasi-CW laser to develop. After factoring in the appropriate time constant, the curves fall back upon themselves. In this experiment, however, the two-peak K-DPAL pulse shape complicated the analysis. It caused the sudden drop and subsequent rise of the efficiency curves seen in Figure 15. It also made it impossible to measure a single slope along the entire length of the curve. Instead, the linear region of the increasing edge was used to determine the efficiency of the K-DPAL. This linear region corresponded to the leading edges of the pump pulse and the K-DPAL pulse. It was the most accurate indicator of the true K-DPAL efficiency because it simultaneously measured the increasing pulse powers while eliminating the effects of the system's

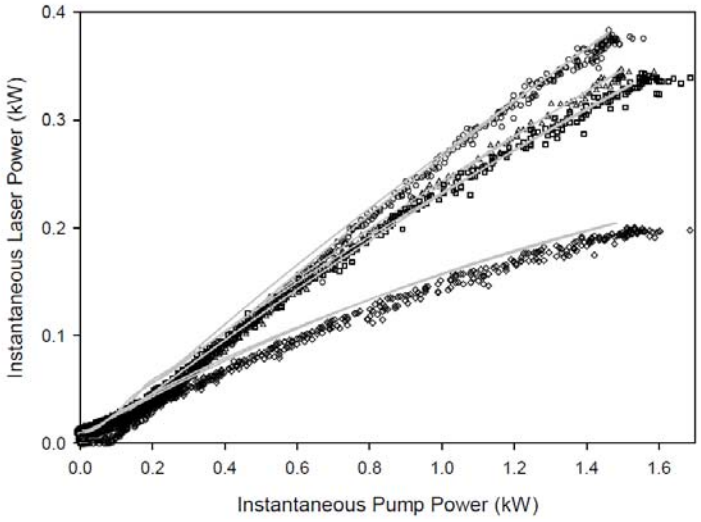

Figure 16. Quasi-CW DPAL Instantaneous Efficiency.
The results from Sulham's pulsed rubidium laser yielded nearly linear instantaneous efficiencies because the pulse duration of 100 ns was long enough for steady state conditions to develop. [3]

impulse response. As discussed before, the efficiency of the K-DPAL was directly related to helium pressure. The effect of pressure on the instantaneous efficiency curves can be seen in Figure 17.

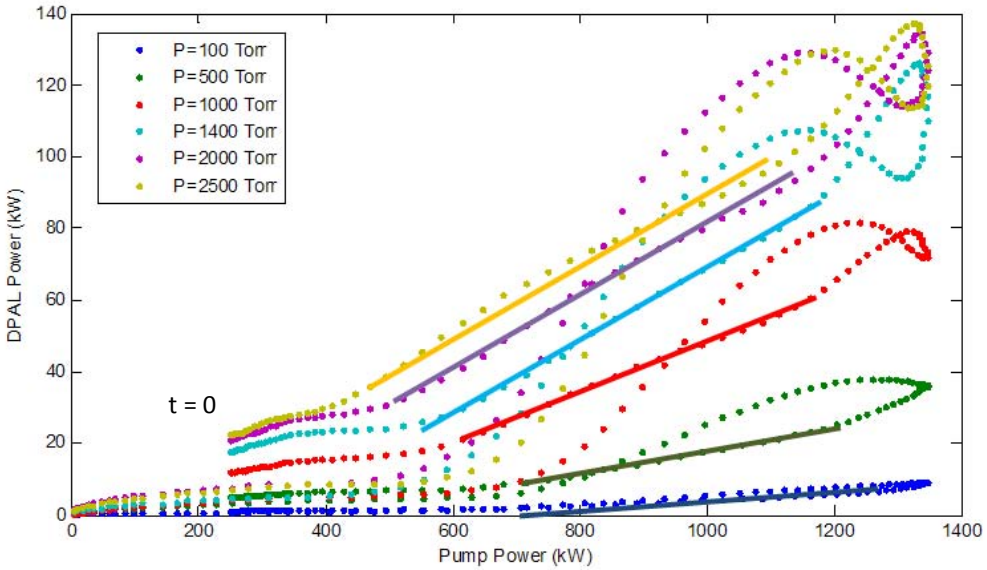

Figure 17. Instantaneous Efficiency vs. Helium Pressure. The K-DPAL efficiency curves were nonlinear due to the short pulse nature of the pump laser. The identified linear regions corresponded to the alignment of the pump and K-DPAL pulse leading edges.

Atomic Recycling

The reason helium pressure increased the efficiency of the K-DPAL was because the atomic recycling rate increased. Each potassium atom was able to absorb more pump photons and emit more K-DPAL photons during a single pump pulse. More specifically, the collisional relaxation rate between the $^2P_{3/2}$ and $^2P_{1/2}$ states increased as described by Equation 14. The rate of absorption on the D_2 line and the rate of stimulated emission on the D_1 line remained constant. Previous work by Wooddy Miller demonstrated that the

maximum DPAL output energy increased with respect to the atomic recycling rate [11]. That DPAL used rubidium vapor collisionally relaxed by ethane. For comparison, Figure 18 is a sample of Miller's results – it shows a near linear increase in pulse energy with respect to the rubidium recycling rate.

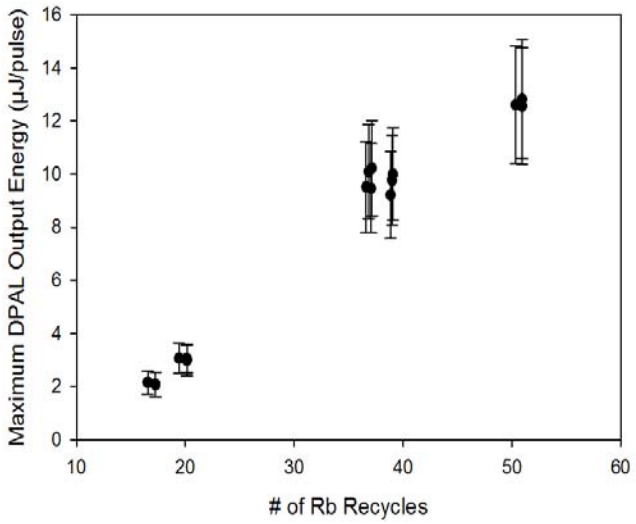

Figure 18. Atomic Recycling in the Pulsed Rb-DPAL .
The results of Miller's work demonstrated a nearly linear relationship between DPAL energy and the number of atomic recycles available during the length of the pulse [11].

The atomic recycling rates in the K-DPAL were similar in magnitude to the Rb-DPAL, though much higher concentrations of buffer gas were needed. The pulse energies were three orders of magnitude higher because the heat pipe generated much higher concentrations of potassium atoms than the standard glass cell used in the Rb-DPAL experiment. In Figure 19, four sample pump powers are displayed. The pulse energies generated by the 95 mW pump power began to roll off as the atomic recycling

rate increased. The curve regained its linearity with higher pump powers thanks to the increased pulse durations and ability to keep the potassium vapor bleached longer.

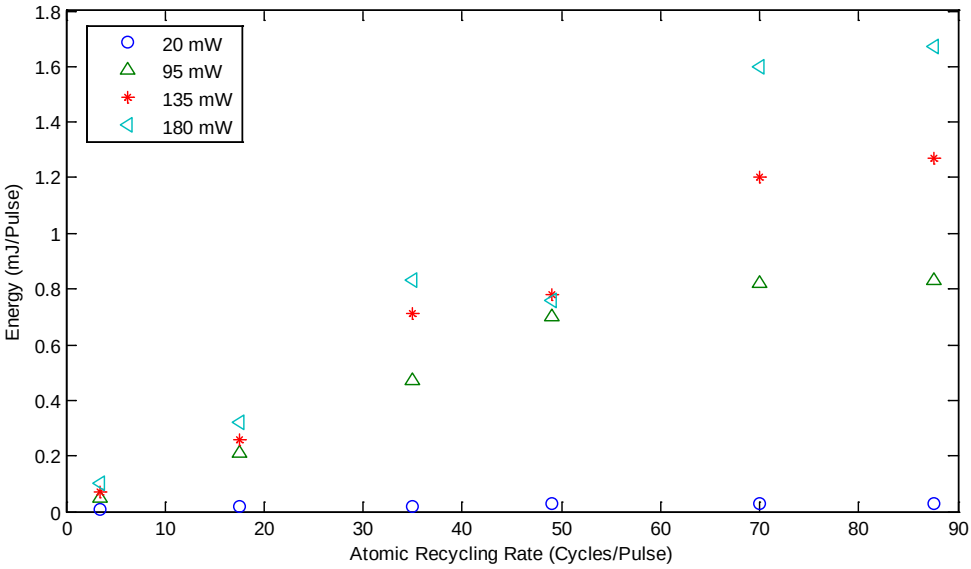

Figure 19. Atomic Recycling in the Pulsed K-DPAL.
The number of cycles per pulse was directly related to helium pressure. An increase in DPAL energy was evident as pump power and pulse duration increased.

Stimulated Raman Scattering

Early in the course of this research, a K-DPAL was attempted using zero helium pressure with the heat pipe raised to 320ºC. The idea was to see if K-K collisions could be used for spin-orbit relaxation. Instead of finding a signal from the D_1 line on the spectrometer, the scattered light from the pump laser was visible on the D_2 line as well as an unexplained line higher in frequency than the pump. The distance between the two lines was the same as the spin-orbit separation. After further investigation, the results seen in Figure 20 were obtained.

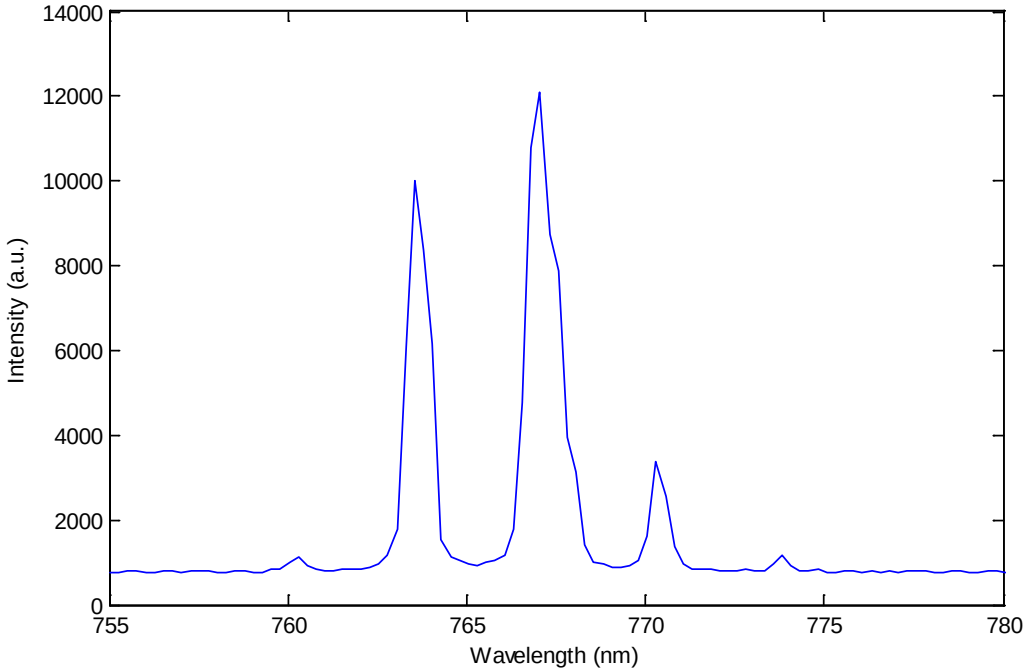

Figure 20. Stimulated Raman Scattering in Potassium Vapor. First and second order Stokes and anti-Stokes lines were found while pumping on the D_2 line with 0 torr of helium pressure. First order scattering was also visible while pumping off line center.

The five spectral lines seen in Figure 20 can be readily explained as stimulated electronic Raman scattering; a specific type of SRS utilizing the electronic energy states of atoms instead of the rotational or vibrational energy states of molecules. The following is a brief explanation of each spectral line. The center line was scattered light from the pump laser on the D_2 line. The high intensity line to its left was the anti-Stokes centered at 763.4 nm. The low intensity line on the far left was the second order anti-Stokes line centered at 760.1 nm. The first line to the right of the pump was the D_1 line and simultaneously the Stokes line. They had the same frequency but were emitted through different processes. The line to the far right is the second order Stokes line

centered at 773.7 nm. Each one of these lines can be explained using the virtual energy levels seen in Figure 21.

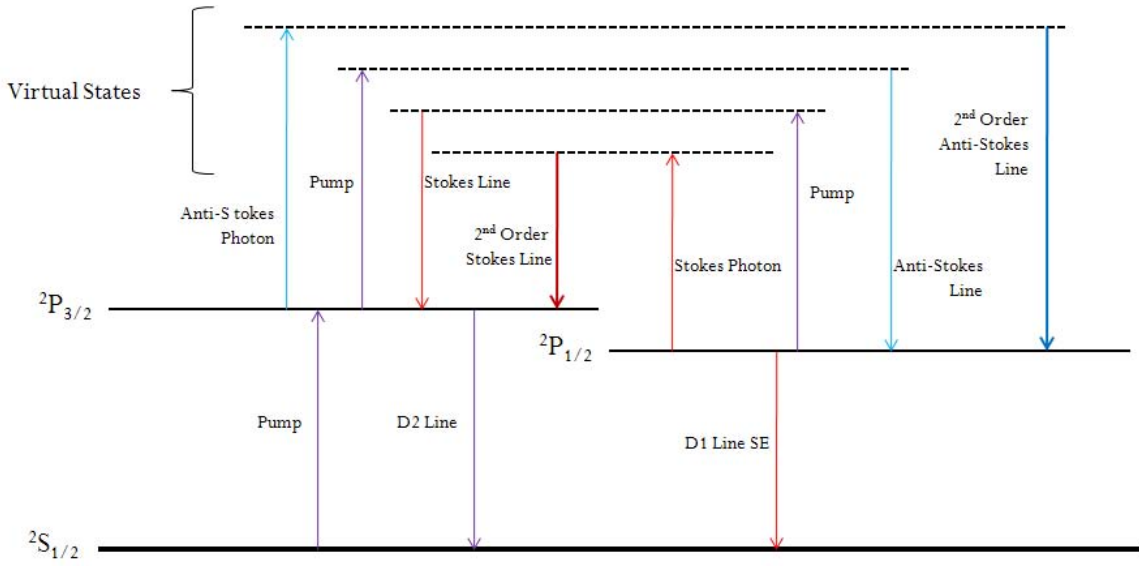

Figure 21. Potassium SRS Energy Level Diagram.
This theoretical description of the SRS system dynamics used first order Stokes and anti-Stokes photons to pump the second order photons through four different virtual energy states.

Stimulated Raman scattering in potassium vapor also occurred when the pump laser was off resonance with the D_2 line. A combination of the D_2 line's large absorption feature and the wide spectral plateau of the dye laser meant that the $^2P_{3/2}$ state was still being pumped, even when the center wavelength of the pump laser was as far as 3 nm from the potassium D_2 line. The Stokes and anti-Stokes lines were offset from the pump line and not the D_2 line. Second order Stokes and anti-Stokes lines were not visible. Similar effects could also be found while pumping the D_1 line. However, only Stokes lines could be generated because of the lower pump frequencies. This data is in strong agreement with the work accomplished by D. J. Bradley in 1970 [12].

V. Conclusions

Conclusions of Research

The results of this thesis will benefit the diode pumped alkali community, especially those researchers using high temperatures and/or high buffer gas pressures in their systems. At these temperatures and pressures, the already large cross section for absorption of the potassium D_2 line yields an extremely large absorption feature. This feature could prove very useful when pumping a DPAL with commercially available diode lasers. If all the pump photons can be used to excite the potassium atoms to the $^2P_{3/2}$ state, then the efficiency of the DPAL will increase significantly.

The high intensity pulsed laser used in this thesis simulated the intensity of a weapons grade DPAL, if only for a few nanoseconds at a time. The large concentration of alkali atoms and the very fast atomic recycling rate proved capable of handling these very high intensities. The heat pipe configuration of this system provided many other advantages. The potassium vapor was confined to the hot region of the heat pipe and could not condense on the optical windows. The long length of the gain medium was able to absorb nearly all the pump photons. Most importantly, the heat pipe could hold the high pressures of helium needed to reach the peak efficiencies found in this thesis research.

Recommendations for Future Research

A better understanding of the cesium, rubidium, and potassium D_2 absorption features for high temperatures and pressures would be essential to the DPAL community. The results should be compared to the line shapes of COTS high power diode lasers. If

the spectral overlap was good, then no further development of diodes would be required for the weapons grade DPAL effort.

The effect of the heat pipe on the fluid dynamics of alkali vapor is currently being studied by Charles Fox using low power CW lasers. This work should be extended to high power CW lasers at high temperatures and pressures to discover if a significant fraction of alkali vapor moves off the lasing axis. If so, a DPAL could be optimized to fill the entire gain medium, thereby creating a small gradient and reducing the movement of alkali vapor away from the lasing axis.

Designs for a transversely pumped, scalable heat pipe should be developed. This heat pipe would allow multiple diode or fiber lasers to be placed along the beam path and optically pump the system. However, the beam quality from a laser cavity with heavy turbulence in the gain medium (such as in a heat pipe) would likely be very poor. A better solution might be to use the heat pipe as an optical amplifier. A high beam quality seed laser could be passed through the amplifier after it has been adjusted for the turbulence in the heat pipe using adaptive optics. The resulting laser would have both high intensity and high beam quality.

Stimulated Raman scattering could prove to be an issue for very low pressure DPALs where the cross sectional rate of SRS is greater than the spin-orbit relaxation rate. Future work should focus on finding these rates as well as the threshold intensity for SRS in cesium, rubidium, and potassium.

Appendix A. K-DPAL Data and Figures

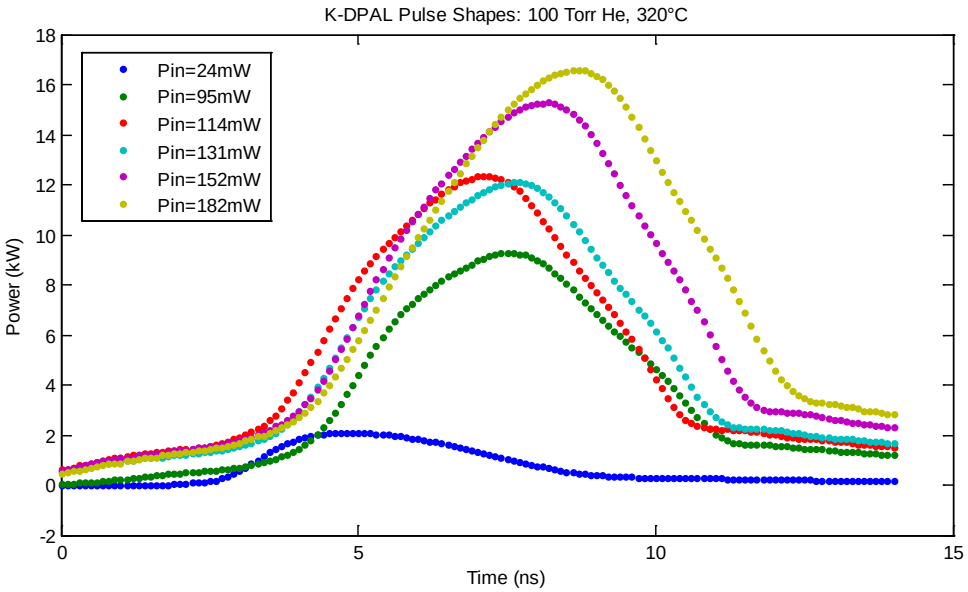

Power Out	Average Efficiency
0.1 mW	0.50%
0.5 mW	0.53%
0.7 mW	0.61%
0.7 mW	0.52%
0.9 mW	0.60%
1.0 mW	0.56%

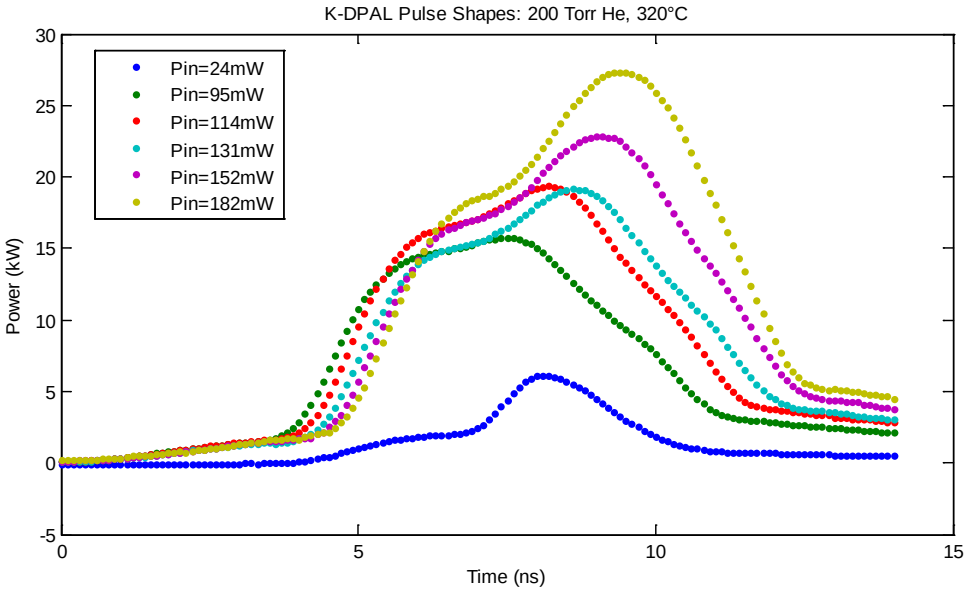

Power Out	Average Efficiency
0.2 mW	1.00%
0.9 mW	0.95%
1.1 mW	0.96%
1.1 mW	0.81%
1.3 mW	0.87%
1.5 mW	0.83%

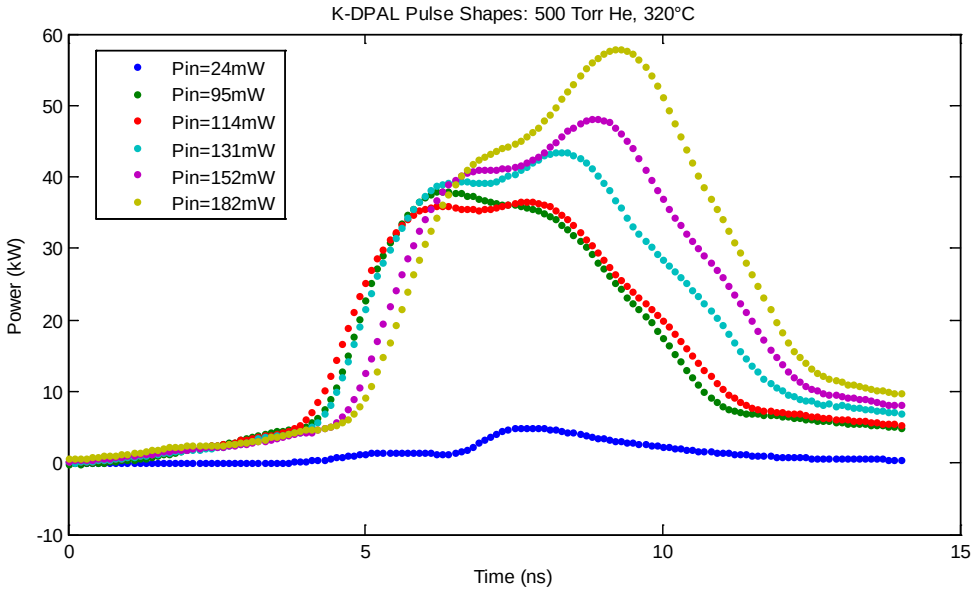

Power Out	Average Efficiency
0.2 mW	1.00%
2.1 mW	2.21%
2.2 mW	1.91%
2.6 mW	1.93%
2.8 mW	1.87%
3.2 mW	1.78%

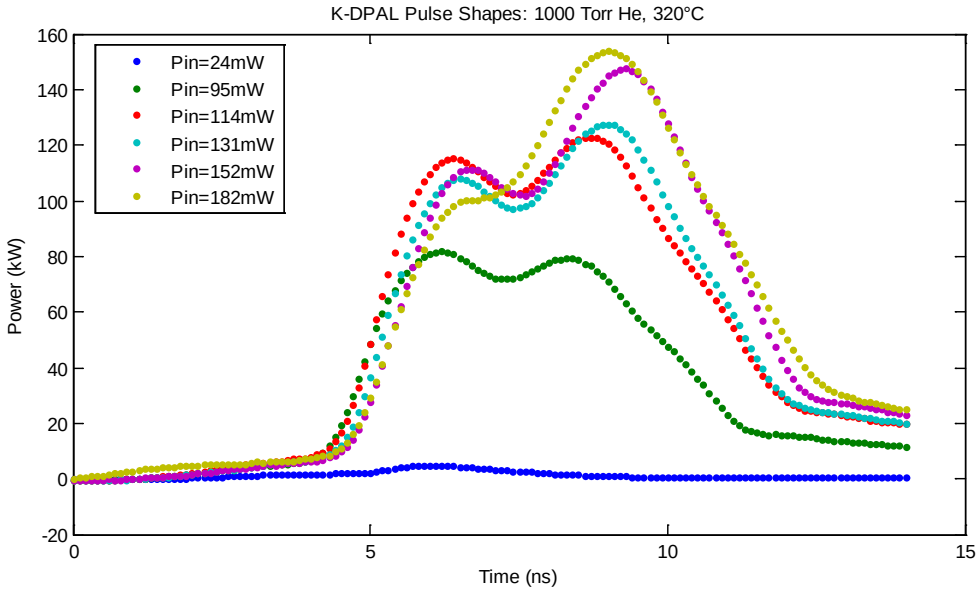

Power Out	Average Efficiency
0.2 mW	1.00%
4.7 mW	4.95%
7.2 mW	6.26%
7.1 mW	5.26%
7.9 mW	5.27%
8.3 mW	4.61%

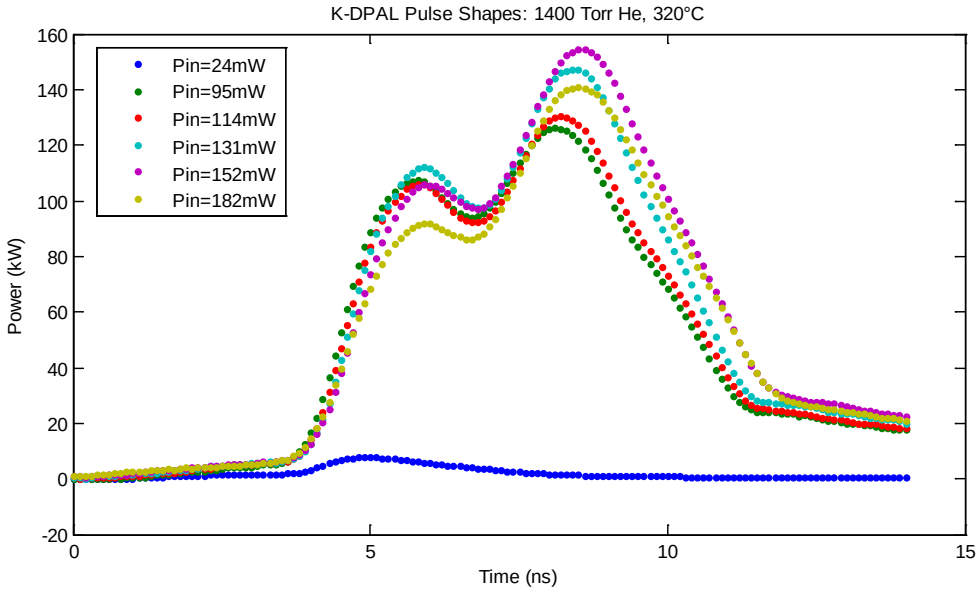

Power Out	Average Efficiency
0.3 mW	1.50%
7.0 mW	7.37%
7.1 mW	6.17%
7.8 mW	5.78%
8.2 mW	5.47%
7.6 mW	4.22%

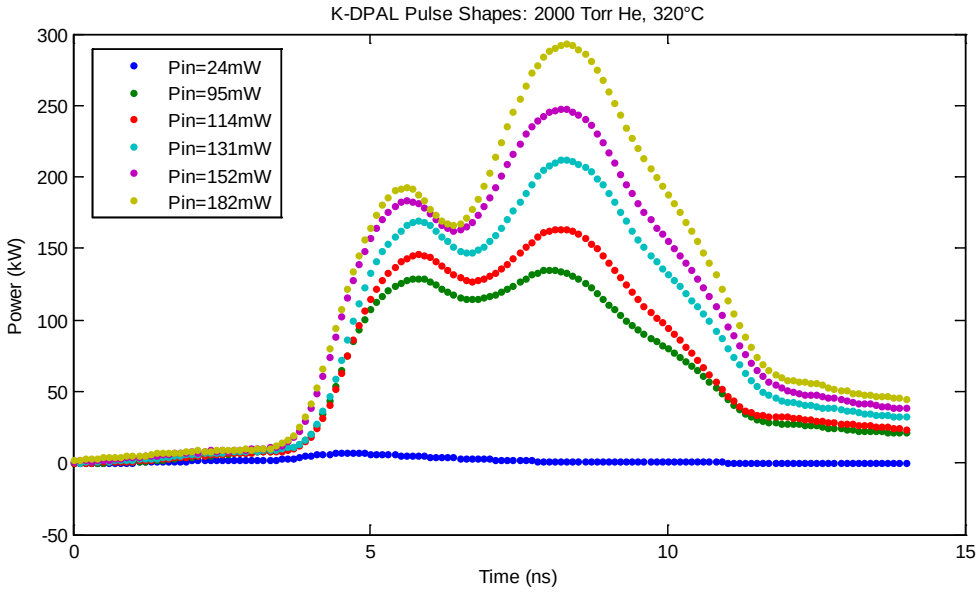

Power Out	Average Efficiency
0.3 mW	1.50%
8.2 mW	8.63%
9.4 mW	8.17%
12.0 mW	8.89%
14.1 mW	9.40%
16.0 mW	8.89%

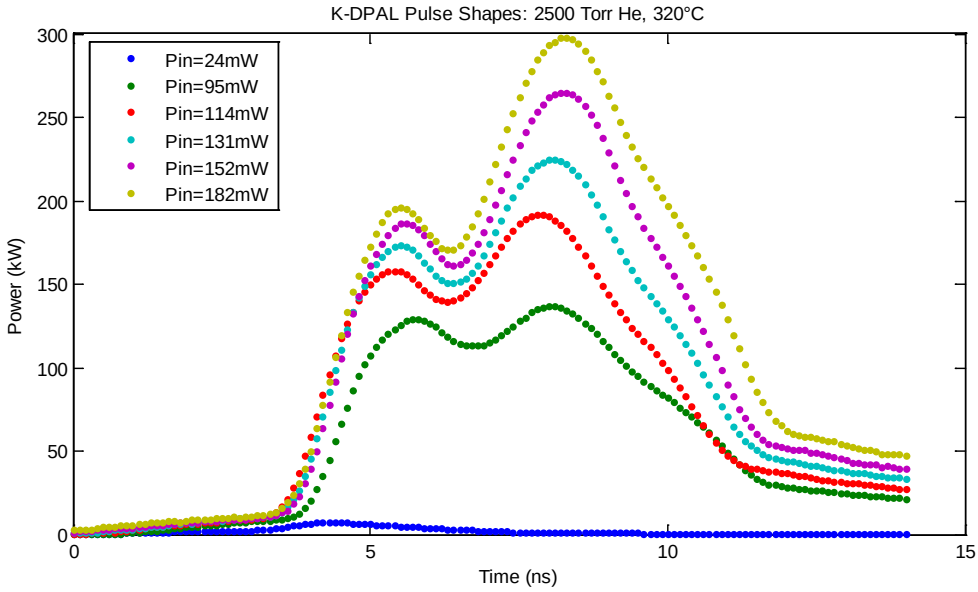

Power Out	Average Efficiency
0.3 mW	1.50%
8.3 mW	8.74%
11.0 mW	9.57%
12.7 mW	9.41%
14.5 mW	9.67%
16.7 mW	9.28%

Bibliography

[1] Glen P. Perram, Salvatore J. Cusumano, Robert L. Hengehold, and Steven T. Fiorino, *An Introduction to Laser Weapon Systems*., 2010.

[2] William F. Krupke, Raymond J. Beach, V. Keith Kanz, and Stephen A. Payne, "Resonance transition 795-nm rubidium laser," *OPTICS LETTERS / Vol. 28, No. 23*, pp. 2336-2338, 2003.

[3] Clifford V. Sulham, "Laser Demonstation and Performance Characterization of Optically Pumped Alkali Laser Systems," Wright Patterson AFB, OH, Dissertation 2010.

[4] Joseph T. Verdeyen, *Laser Electronics, 3rd ed.* Upper Saddle River, NJ: Prentice Hall, 2000.

[5] T. G. Tiecke, "Properties of Potassium," University of Amsterdam, The Netherlands, Thesis 2010.

[6] Greg A. Pitz, "Collisional Dynamics of the Cesium D1 and D2 Transitions," Air Force Institute of Technology, Wright Patterson AFB, OH, Dissertation 2010.

[7] L. Kraus, "Collisional Excitation Transfer Between the 2P1/2 and 2P3/2 Levels in Alkali Atoms," *Applied Optics*, vol. 5, no. 9, pp. 1375-1382, September 1966.

[8] Newport. (2008) Technical Report. [Online]. http://www.newport.com/images/webDocuments-EN/images/11810.pdf

[9] Natl. Inst. Stand. Technol., Revised Thermocouple Reference Tables: Type J , 1993.

[10] Gordon Hager, Personal Correspondence, 2010.

[11] Wooddy S. Miller, "Rubidium Recycling in a High Intensity Short Pulsed Alkali Laser," Wright Patterson AFB, OH, 2010.

[12] D. J. Bradley, G. M. Gale, and P. D. Smith, "Stimulated Stokes and anti-Stokes electronic Raman scattering by selectively excited potassium and rubidium atoms," 1971.

[13] Jason Zweiback, Gordon Hager, and William F. Krupke, "High efficiency hydrocarbon-free resonance transition potassium laser," *Optics Communications 282*, pp. 1871-1873, 2009.

[14] Newport. (2010) Technical Report. [Online]. http://www.newport.com/images/webDocuments-EN/images/14773.pdf

[15] Wikipedia. (2010) Wikipedia. [Online]. http://en.wikipedia.org/wiki/Raman_scattering

Vita

Captain Edward J. Hurd, Jr. is a student at the Air Force Institute of Technology, Wright-Patterson AFB, OH. He is working towards a Master of Science in Electrical Engineering with a specialty in Electro-Optics. His area of research is diode pumped alkali lasers with a focus on pulsed, potassium vapor lasers. Following graduation, he will be assigned to the Air Force Research Laboratory's Sensors Directorate.

Captain Hurd entered the Air Force in 2004 after graduating from the United States Air Force Academy with a Bachelor of Science in Computer Engineering. In 2008, he graduated from Oklahoma City University with a Master of Business Administration. While at Tinker AFB, OK, Captain Hurd served as a facility and process engineer for the 76th Commodities Maintenance Group and as an avionics engineer for the KC-10 Program Office. He earned his Lean, 6-Sigma Green Belt for his work with Local Manufacturing at Tinker AFB.

REPORT DOCUMENTATION PAGE

Form Approved
OMB No. 074-0188

1. REPORT DATE *(DD-MM-YYYY)*	**2. REPORT TYPE**	**3. DATES COVERED** *(From – To)*
24-03-2011	Master's Thesis	August 2010 – March 2011

4. TITLE AND SUBTITLE

Characteristics of a High Intensity, Pulsed, Potassium Vapor Laser in a Heat Pipe

5a. CONTRACT NUMBER

5b. GRANT NUMBER

5c. PROGRAM ELEMENT NUMBER

6. AUTHOR(S)

Hurd, Edward J. Jr, Captain, USAF

5d. PROJECT NUMBER

5e. TASK NUMBER

5f. WORK UNIT NUMBER

7. PERFORMING ORGANIZATION NAMES(S) AND ADDRESS(S)

Air Force Institute of Technology
Graduate School of Engineering and Management (AFIT/EN)
2950 Hobson Way, Building 640
WPAFB OH 45433-8865

8. PERFORMING ORGANIZATION REPORT NUMBER

AFIT/GE/ENG/11-17

9. SPONSORING/MONITORING AGENCY NAME(S) AND ADDRESS(ES)

Intentionally Left Blank

10. SPONSOR/MONITOR'S ACRONYM(S)

11. SPONSOR/MONITOR'S REPORT NUMBER(S)

12. DISTRIBUTION/AVAILABILITY STATEMENT

APPROVED FOR PUBLIC RELEASE; DISTRIBUTION UNLIMITED.

13. SUPPLEMENTARY NOTES

14. ABSTRACT

This thesis research paper presents the results of experiments using an optically pumped, pulsed potassium vapor laser in a heat pipe. The absorption on the potassium D_2 line, output laser characteristics, and Raman scattering in potassium vapor are discussed. The spectral full width at half maximum (FWHM) of the D_2 absorption line was much greater than predicted values for pressure broadening due to the high number density of potassium atoms and the long path length. At 320°C and 0 torr of helium, the FWHM was 765 GHz. At 100 torr it was 968 GHz. At 200 torr it was 1.12 THz. The analyzed potassium laser output characteristics include the temporal dynamics of the laser cavity, the instantaneous energy efficiencies, and the spin-orbit recycling rates. At 320°C with 2500 torr of helium, a potassium laser with 1.53 MW/cm^2 peak intensity and 8.25% slope efficiency was demonstrated. At 320°C and 0 torr of helium, stimulated electronic Raman scattering occurred in the potassium heat pipe. First and second order Stokes and anti-Stokes lines were visible with energy differences identical to the spin-orbit splitting of potassium.

15. SUBJECT TERMS

DPAL, Potassium, Heat Pipe, Raman Scattering, SRS, SERS

16. SECURITY CLASSIFICATION OF:			**17. LIMITATION OF ABSTRACT**	**18. NUMBER OF PAGES**	**19a. NAME OF RESPONSIBLE PERSON**
a. REPORT	**b. ABSTRACT**	**c. THIS PAGE**			Jeremy C. Holtgrave, Lt Col, USAF
U	U	U	UU	59	**19b. TELEPHONE NUMBER** *(Include area code)* (937) 785-3636, ext 4649 (Jeremy.Holtgrave@afit.edu)

Standard Form 298 (Rev. 8-98)
Prescribed by ANSI Std. Z39-18